1   **Supplement**

2

3

4

5

6

7

8

30 **Figure S1.** Monthly mean concentrations of observed (ICOS) and simulated (BGD and BGD+ANT) CH$_4$ at 10, 50 and 100 m

31 above ground level for all stations. BGD and ANT represent the simulated concentrations from background and anthropogenic

32 sources, respectively. The mean concentrations were computed based on quality-controlled ICOS CH$_4$ data. Contributions from

33 natural sources (wetlands and termites) and biomass burning were not relevant during the study period.
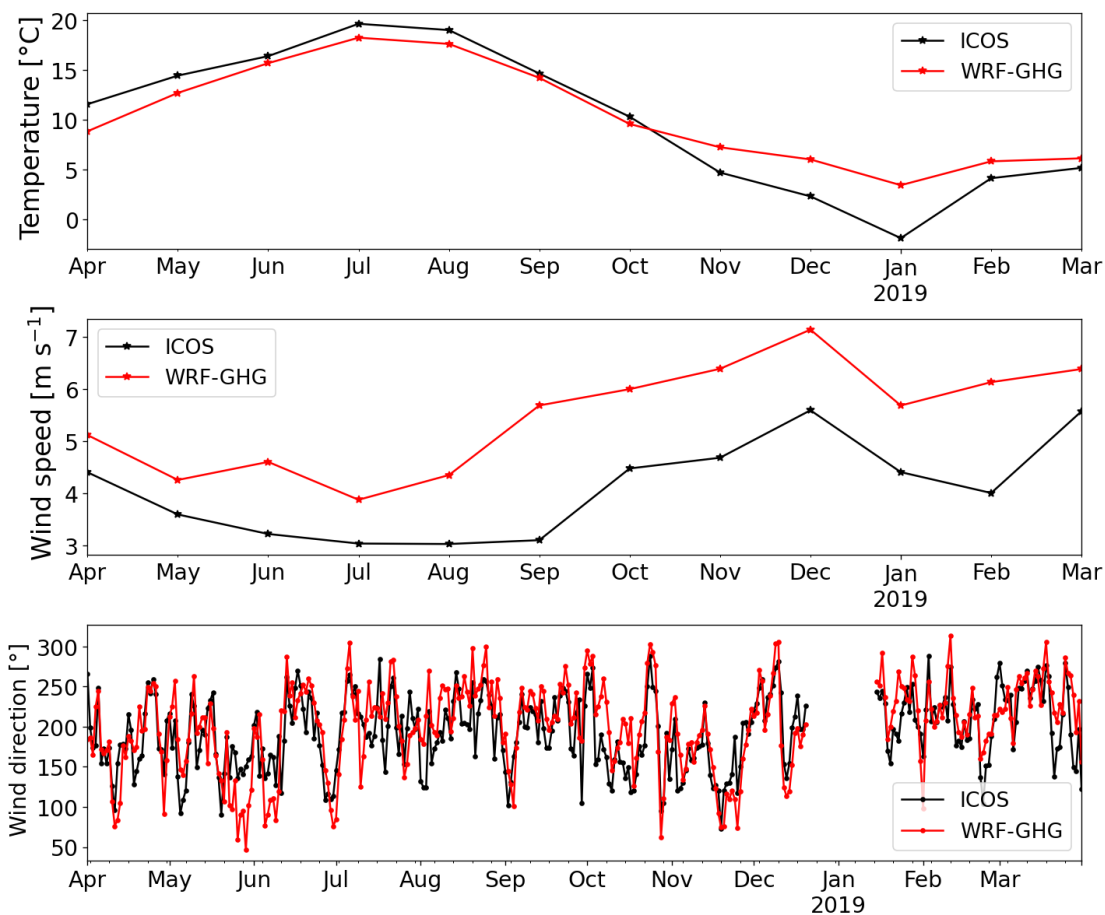
34

35

36

37

38

39

40

1

Figure S2. Monthly (and daily) mean values of observed and simulated temperature, wind speed (and wind direction) at 10 m above ground level. The mean concentrations were computed based on quality-controlled ICOS data.

2

81
82
83
84
85
86
87
88
89
90
91
92
93
94
95
96
97
98
99
100
101
102
103
104
105
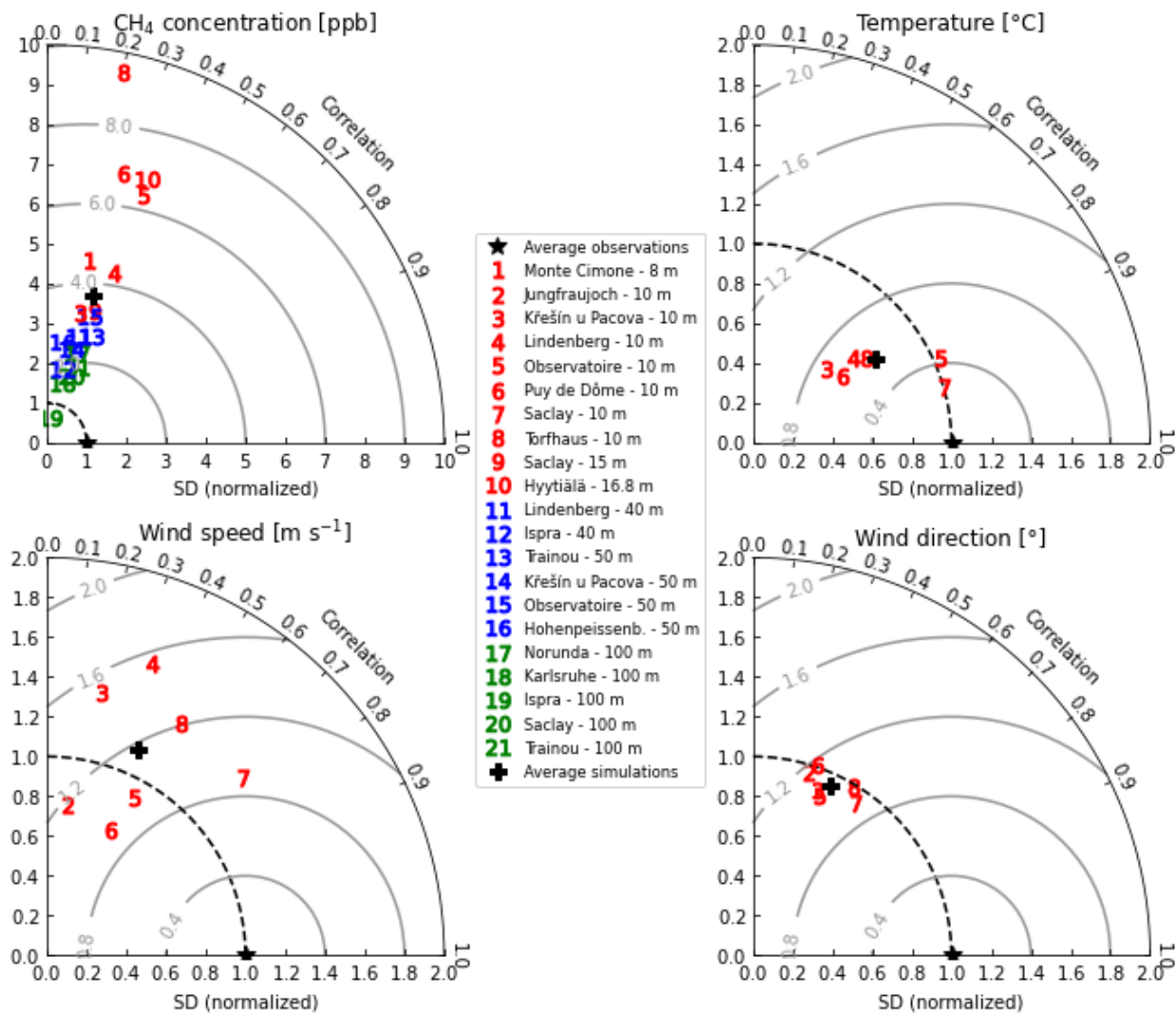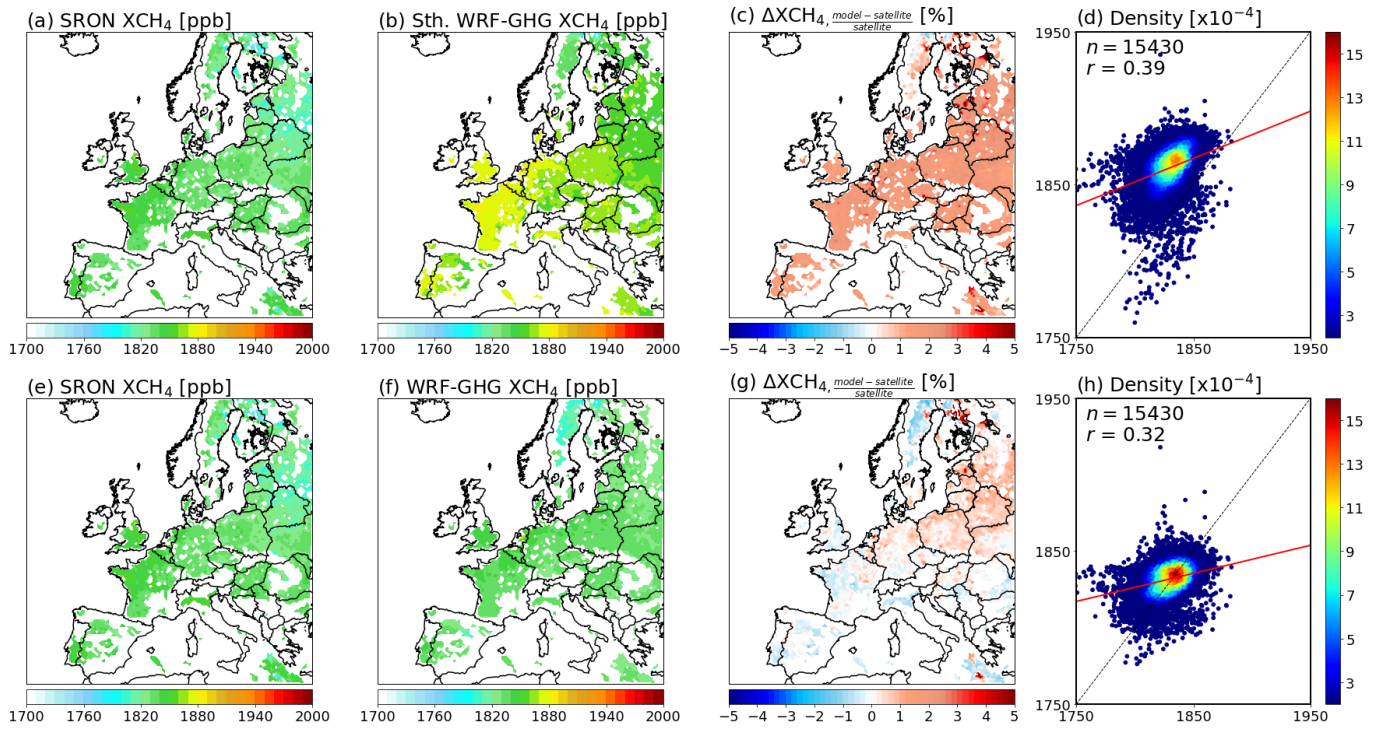106
107
108
109
110
111
112
113
114
115
116
117
118
119
120

Figure S3. Correlation coefficients and standard deviation (SD) model to observation ratios for CH_4 concentrations, temperature, wind speed and wind direction. The numbers in red, blue and green represent ICOS stations with data with sampling heights between 8.0–16.8 m, 40–50 m, and 100 m, respectively (see Table 3 for station details).
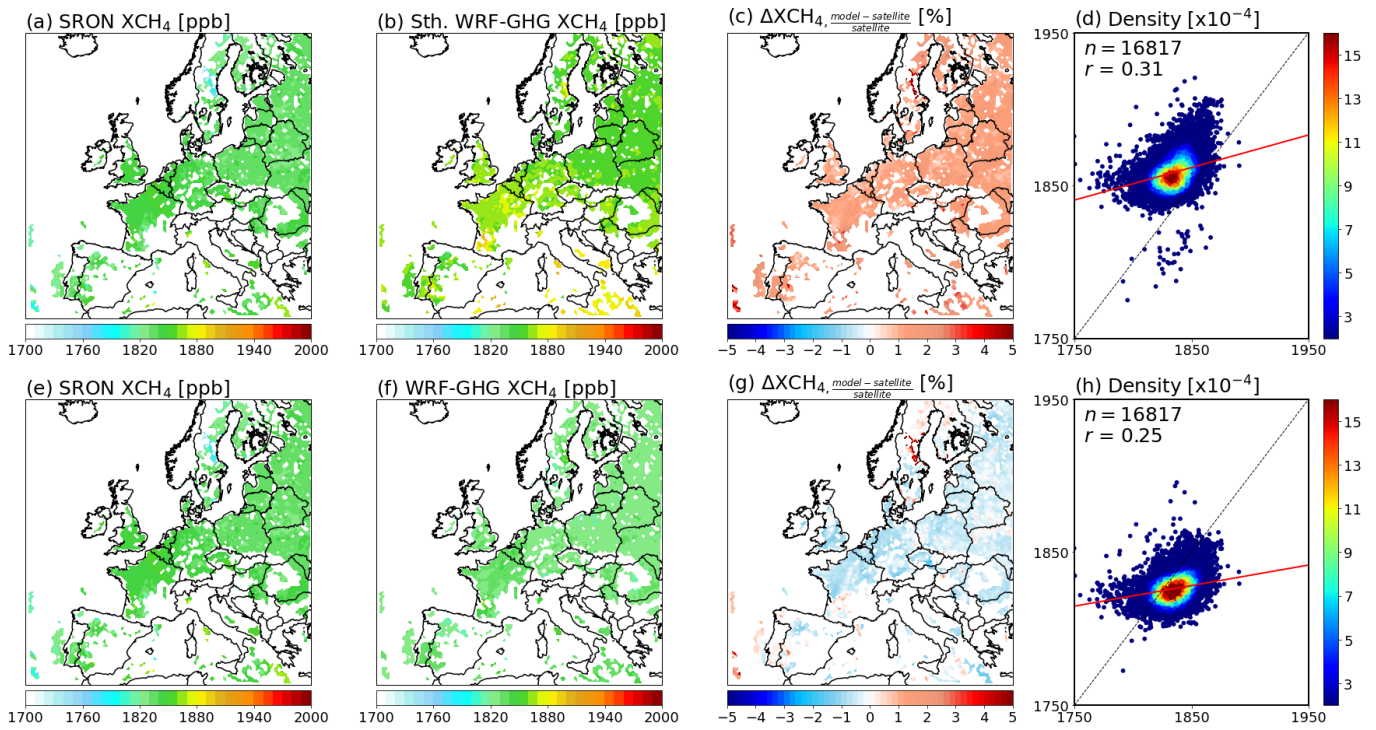
121
122
123
124
125
126
127
128
129

Figure S4. Temporal mean spatial distributions of XCH$_4$ concentration from SRON RemoTeC-S5P (panels a and e) and WRF-GHG estimates with and without smoothing (panels b and f, respectively), along with their relative differences (panels c and g), averaged over the period from April 1 to April 30, 2018.
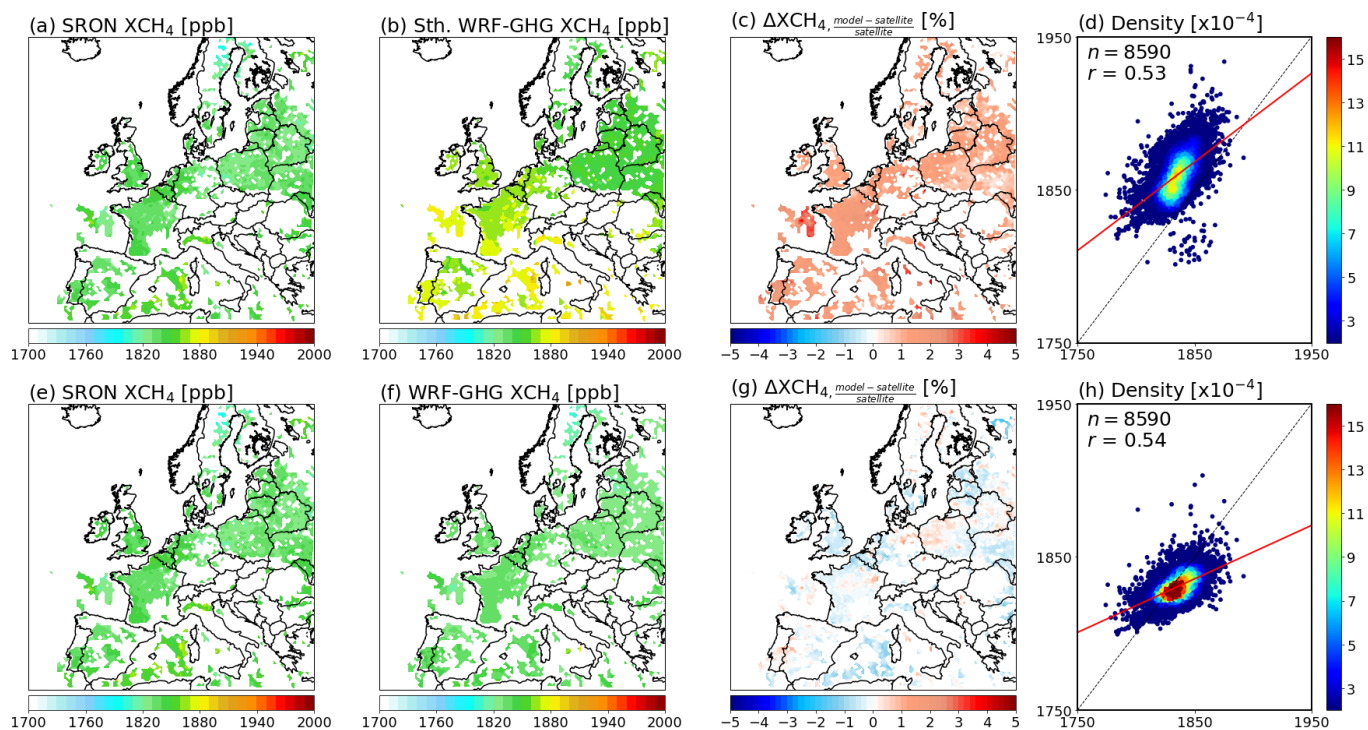
134
135
136
137
138
139
140
141
142
143

4

144

145

146

147

148

149

150

151

Figure S5. Temporal mean spatial distributions of XCH_4 concentration from SRON RemoTeC-S5P (panels a and e) and WRF-GHG estimates with and without smoothing (panels b and f, respectively), along with their relative differences (panels c and g), averaged over the period from May 1 to May 31, 2018.

156

157

158

159

160

161

162

163

164

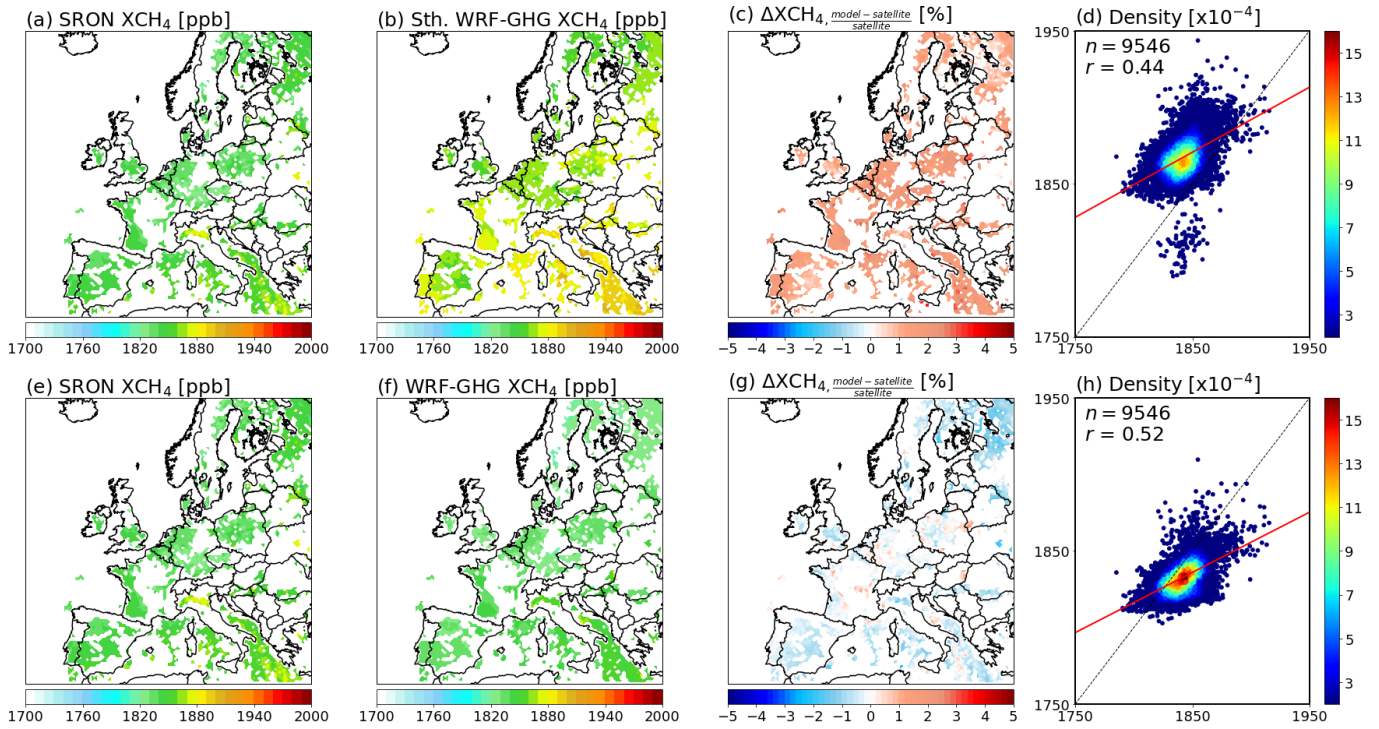165

166

5

167
168
169
170
171
172
173
174

Figure S6. Temporal mean spatial distributions of XCH$_4$ concentration from SRON RemoTeC-S5P (panels a and e) and WRF-GHG estimates with and without smoothing (panels b and f, respectively), along with their relative differences (panels c and g), averaged over the period from June 1 to June 30, 2018.
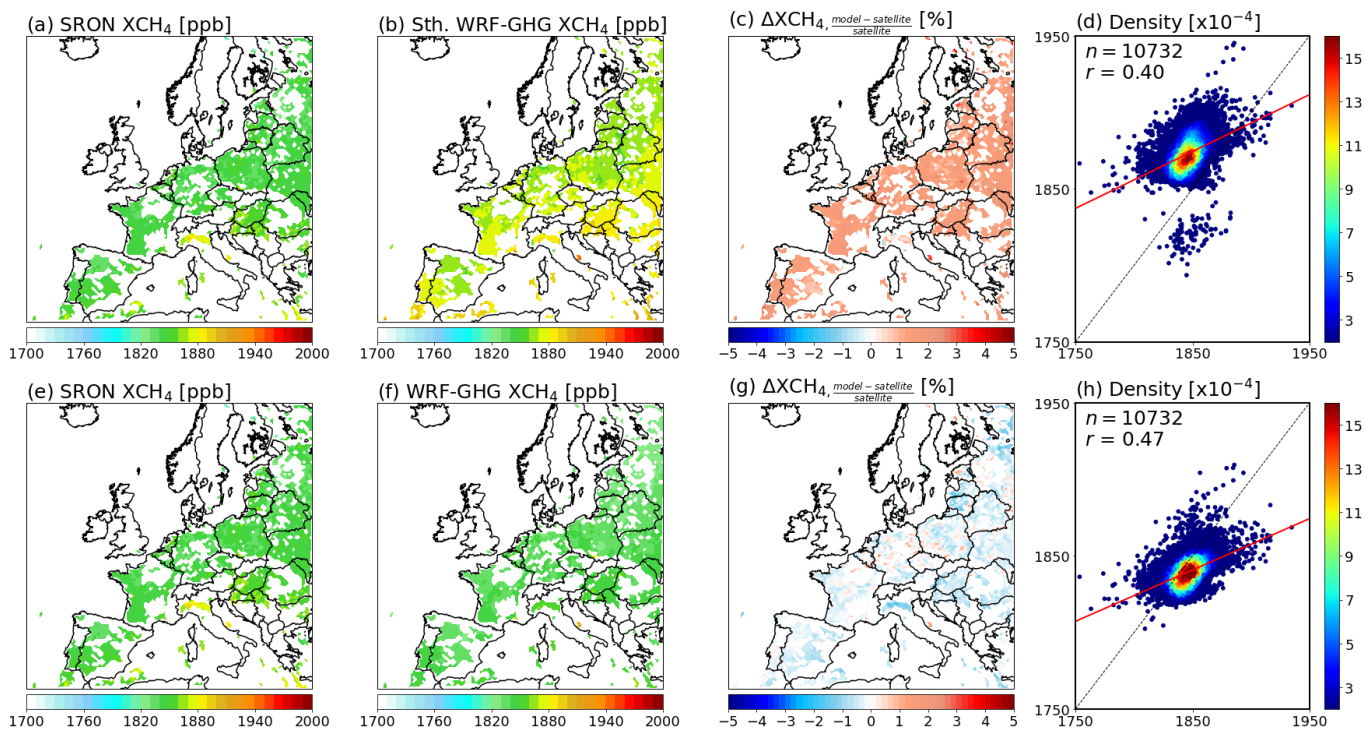
179
180
181
182
183
184
185
186
187
188
189

6

190
191
192
193
194
195
196
197
198
199

Figure S7. Temporal mean spatial distributions of XCH_4 concentration from SRON RemoTeC-S5P (panels a and e) and WRF-GHG estimates with and without smoothing (panels b and f, respectively), along with their relative differences (panels c and g), averaged over the period from July 1 to July 31, 2018.
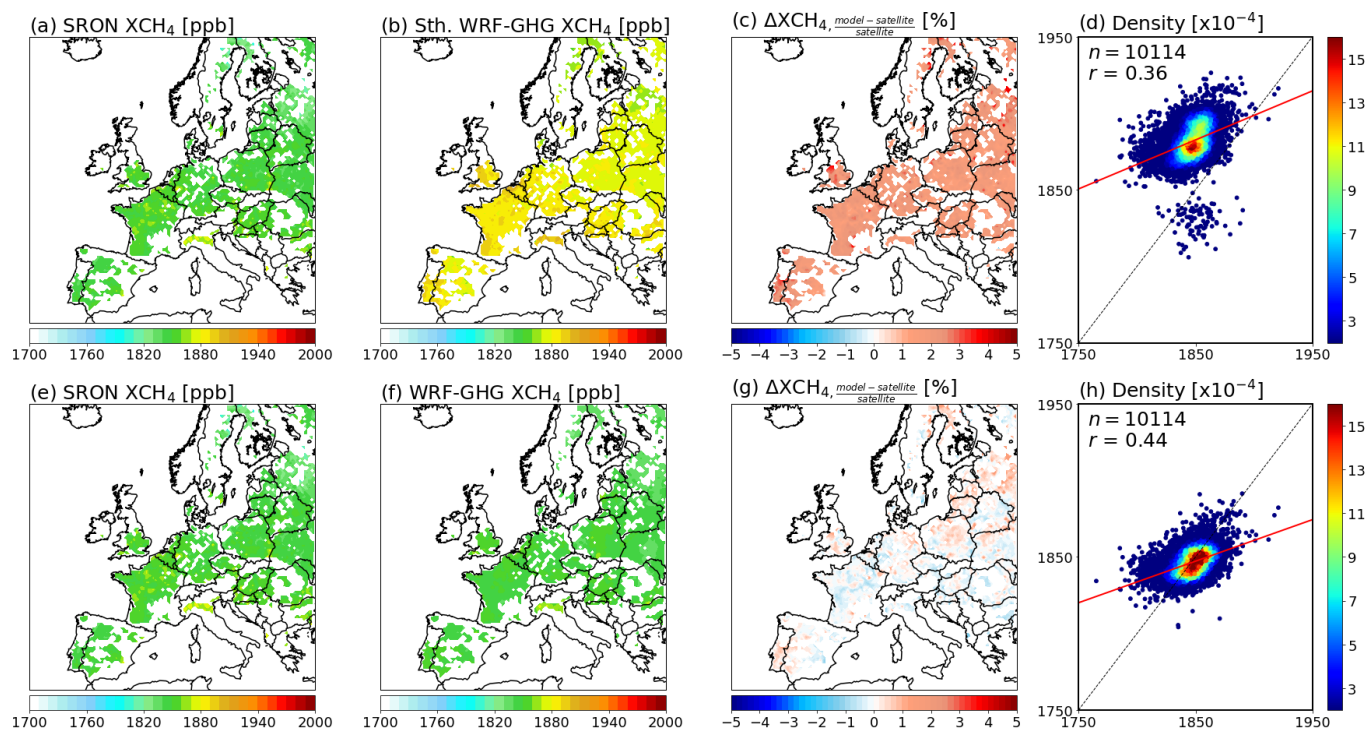
204
205
206
207
208
209
210
211
212

213

214

215

216

217

218

219

220

221

Figure S8. Temporal mean spatial distributions of XCH$_4$ concentration from SRON RemoTeC-S5P (panels a and e) and WRF-GHG estimates with and without smoothing (panels b and f, respectively), along with their relative differences (panels c and g), averaged over the period from August 1 to August 31, 2018.

226

227

228

229

230

231

232

233

234
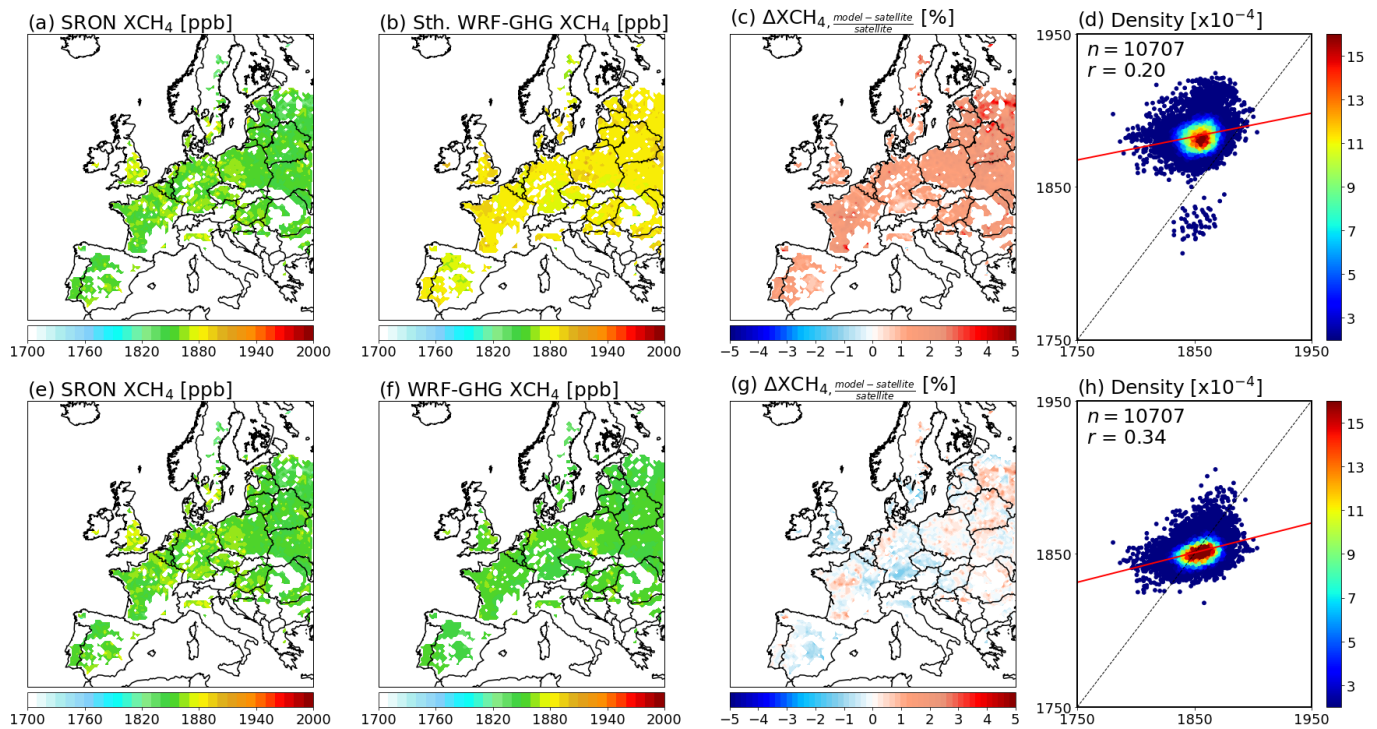
235

236
237
238
239
240
241
242
243
244
245

Figure S9. Temporal mean spatial distributions of XCH_4 concentration from SRON RemoTeC-S5P (panels a and e) and WRF-GHG estimates with and without smoothing (panels b and f, respectively), along with their relative differences (panels c and g), averaged over the period from September 1 to September 30, 2018.
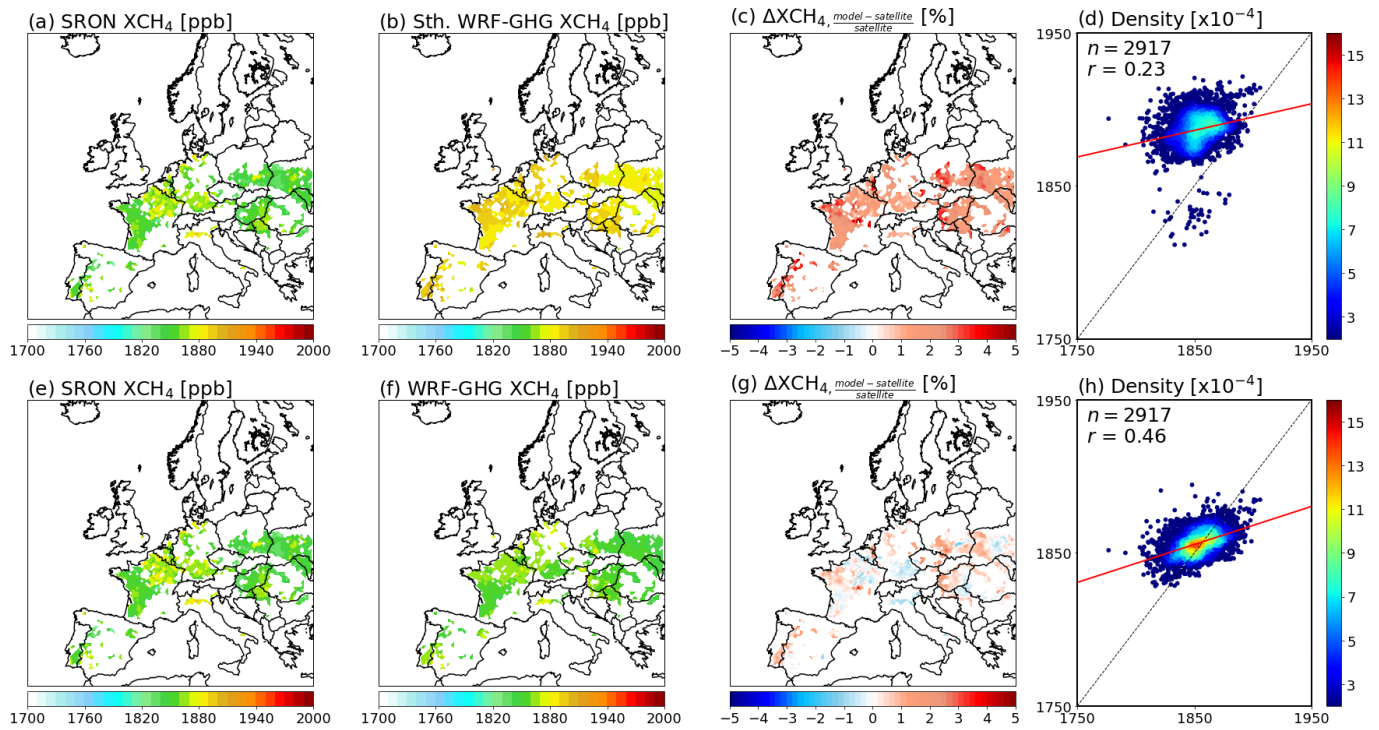
250
251
252
253
254
255
256
257
258

9

259
260
261
262
263
264
265
266
267

Figure S10. Temporal mean spatial distributions of XCH$_4$ concentration from SRON RemoTeC-S5P (panels a and e) and WRF-GHG estimates with and without smoothing (panels b and f, respectively), along with their relative differences (panels c and g), averaged over the period from October 1 to October 31, 2018.
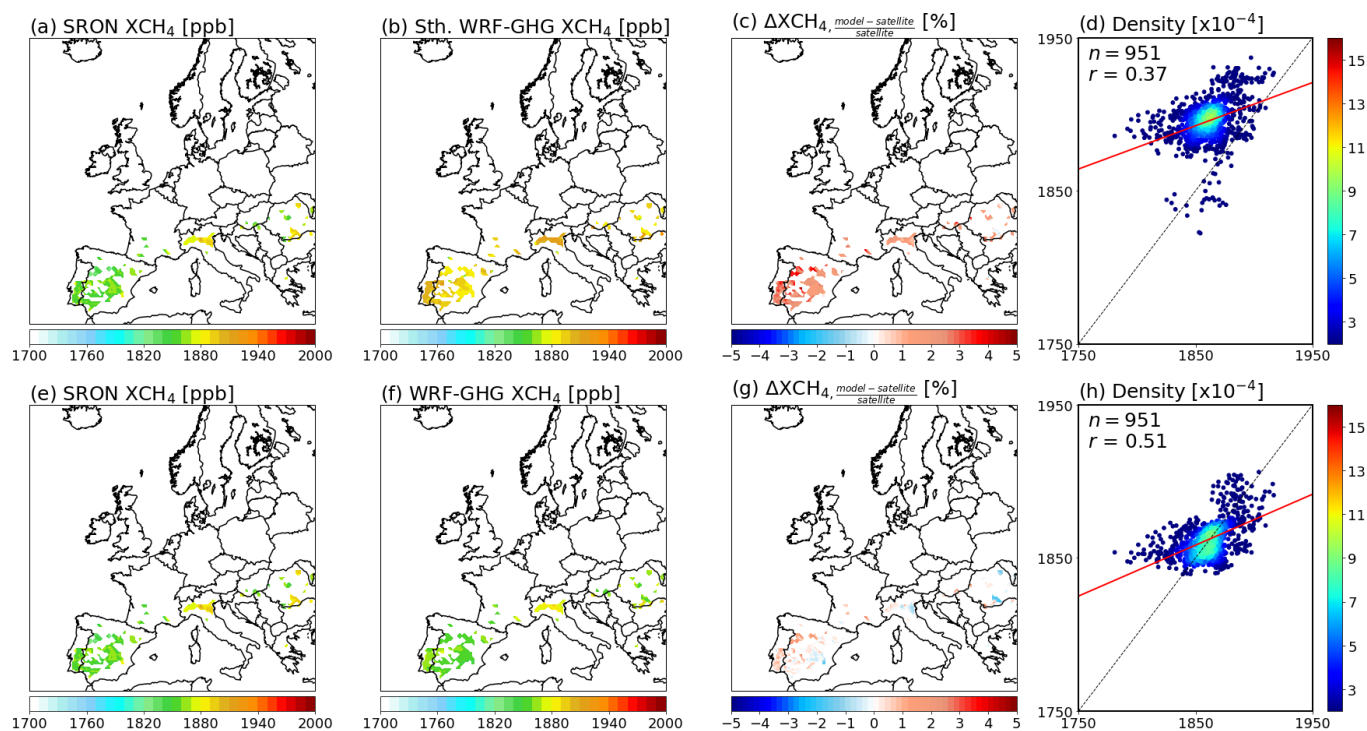
272
273
274
275
276
277
278
279
280
281

10

282
283
284
285
286
287
288
289
290
291

293 **Figure S11.** Temporal mean spatial distributions of XCH_4 concentration from SRON RemoTeC-S5P (panels a and e) and WRF-
294 GHG estimates with and without smoothing (panels b and f, respectively), along with their relative differences (panels c and g),
295 averaged over the period from November 1 to November 30, 2018.
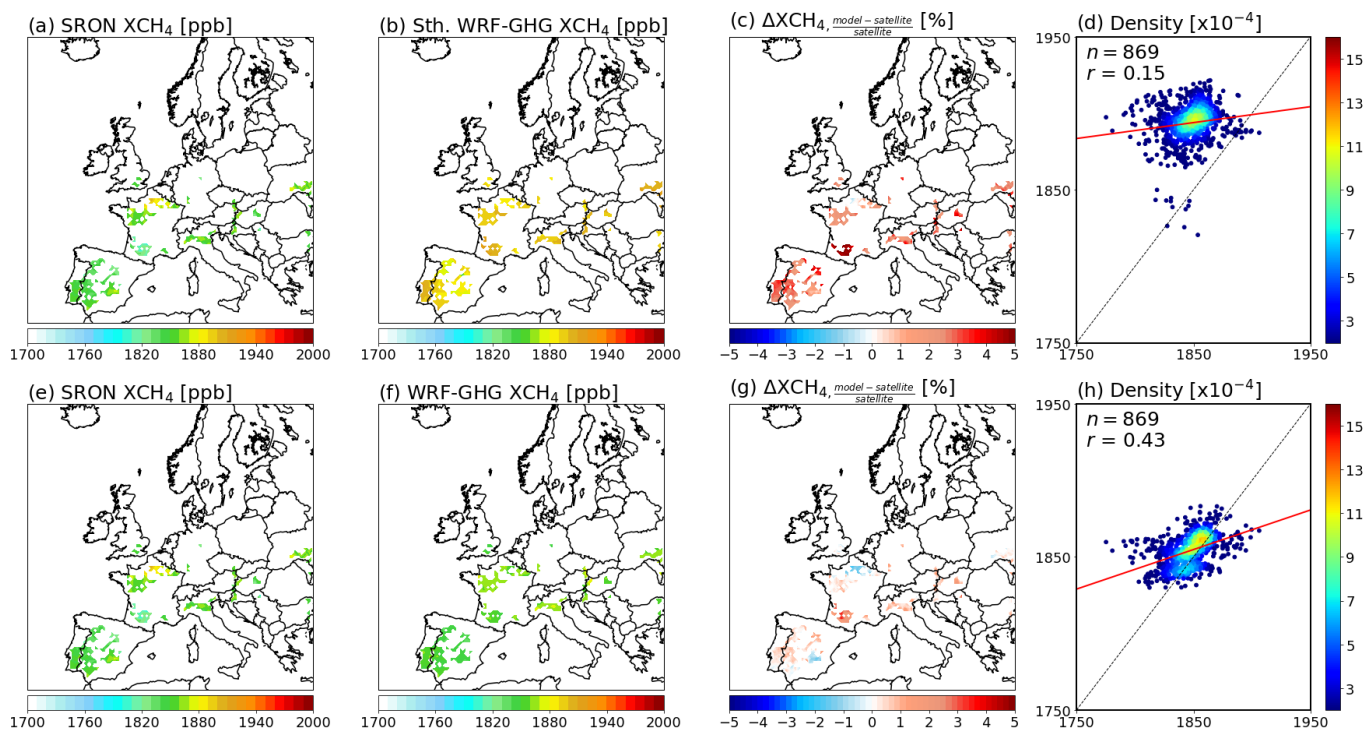
296
297
298
299
300
301
302
303
304

305
306
307
308
309
310
311
312
313
314

Figure S12. Temporal mean spatial distributions of XCH_4 concentration from SRON RemoTeC-S5P (panels a and e) and WRF-GHG estimates with and without smoothing (panels b and f, respectively), along with their relative differences (panels c and g), averaged over the period from December 1 to December 20, 2018.
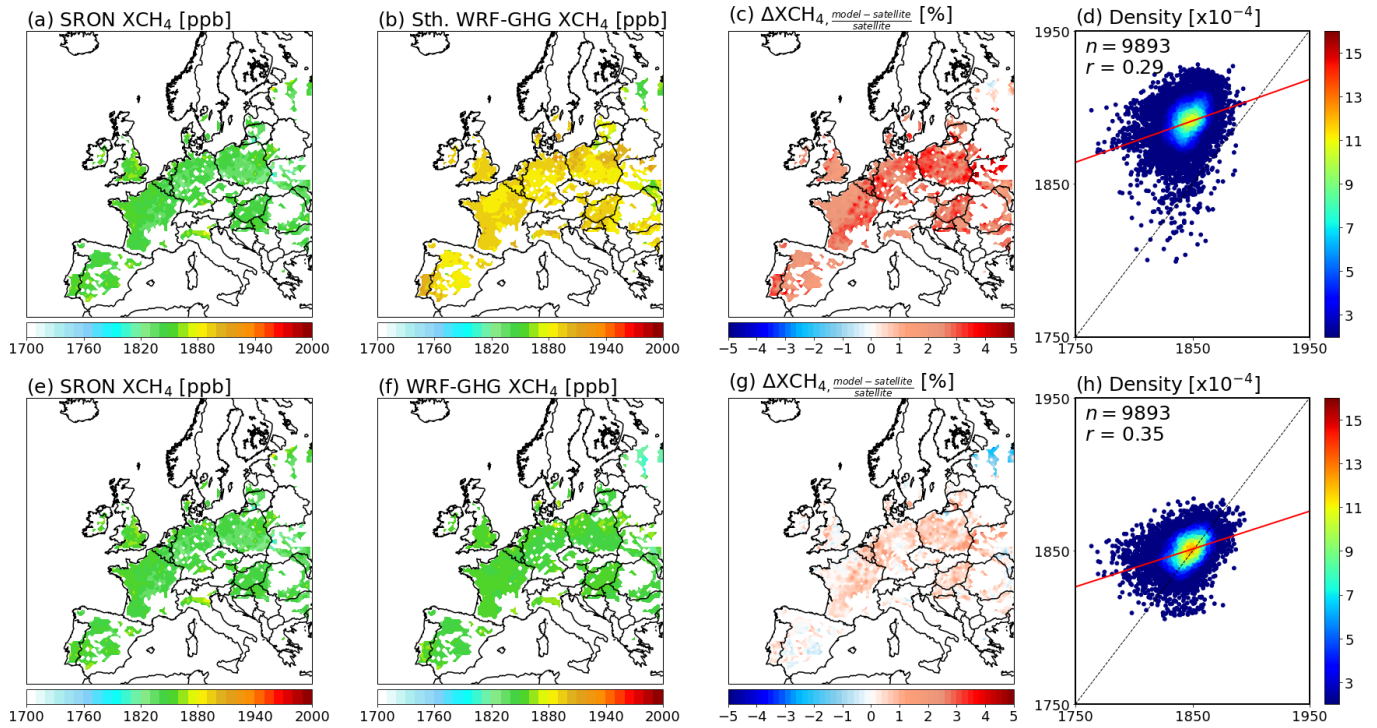
319
320
321
322
323
324
325
326
327

328
329
330
331
332
333
334
335
336
337
338

Figure S13. Temporal mean spatial distributions of XCH$_4$ concentration from SRON RemoTeC-S5P (panels a and e) and WRF-GHG estimates with and without smoothing (panels b and f, respectively), along with their relative differences (panels c and g), averaged over the period from January 15 to January 31, 2019.
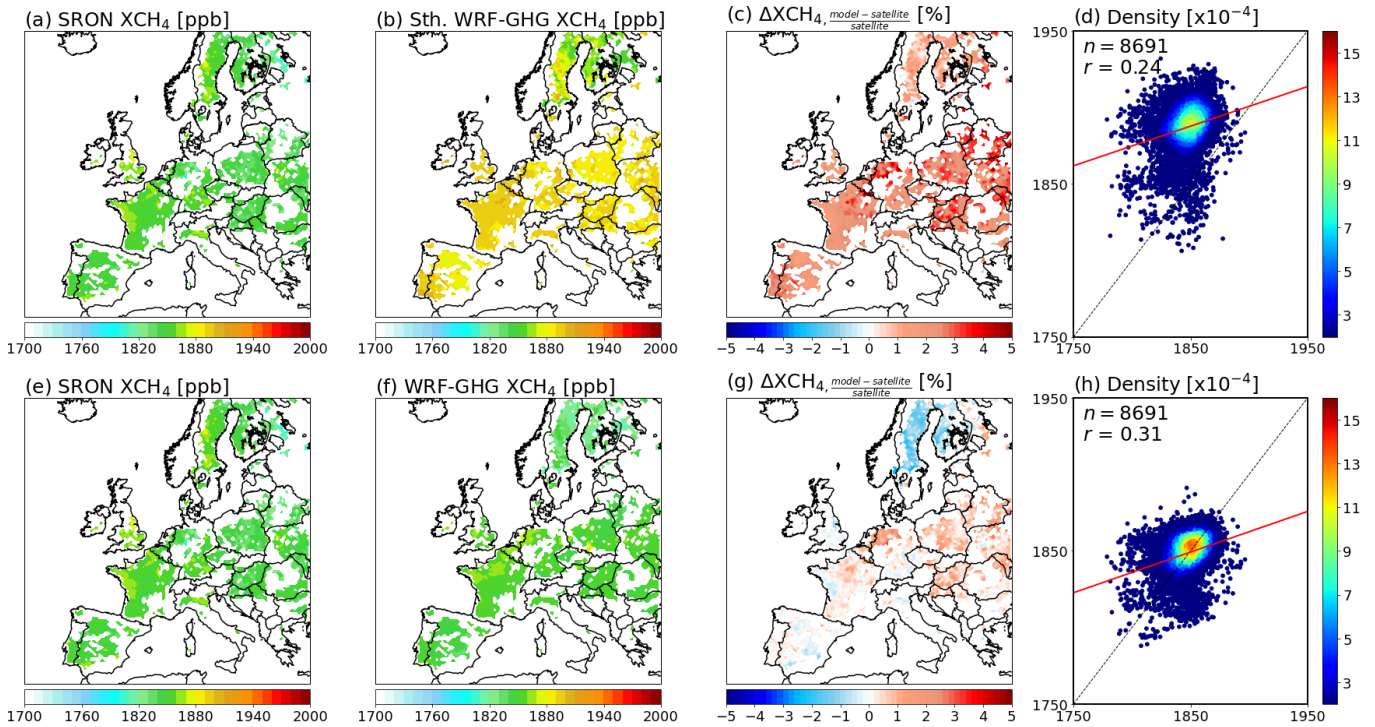
343
344
345
346
347
348
349
350

351
352
353
354
355
356
357
358
359
360

Figure S14. Temporal mean spatial distributions of XCH$_4$ concentration from SRON RemoTeC-S5P (panels a and e) and WRF-GHG estimates with and without smoothing (panels b and f, respectively), along with their relative differences (panels c and g), averaged over the period from February 1 to February 28, 2019.

362
363
364
365
366
367
368
369
370
371
372
373

374
375
376
377
378
379
380
381
382
383
384

Figure S15. Temporal mean spatial distributions of XCH$_4$ concentration from SRON RemoTeC-S5P (panels a and e) and WRF-GHG estimates with and without smoothing (panels b and f, respectively), along with their relative differences (panels c and g), averaged over the period from March 1 to March 31, 2019.

389
390
391
392
393
394
395